High Resolution Quantitative MRI of Multiple Sclerosis Spinal Cord Lesions

Journal:	*Magnetic Resonance in Medicine*
Manuscript ID	MRM-21-22523.R2
Wiley - Manuscript type:	Technical Note
Research Type:	Image processing/Image analysis < Technical Research
Research Focus:	Pathology < Anatomy < Spine and peripheral nerves < Neurological

High Resolution Quantitative MRI of Multiple Sclerosis Spinal Cord Lesions

Amy R McDowell[1], Natalia Petrova[2], Daniele Carassiti[2], Marc E Miquel[3], David L Thomas[4], Gareth J Barker[5], Klaus Schmierer*[2,6], Tobias C Wood*[5]

Affiliations:

[1]Queen Square Centre for Neuromuscular Diseases, UCL, London, UK

[2]The Blizard Institute (Neuroscience, Surgery & Trauma), Queen Mary University of London, Barts and The London School of Medicine & Dentistry, London, UK

[3]Clinical Physics, Barts Health NHS Trust

[4]Department of Brain Repair and Rehabilitation, UCL Queen Square Institute of Neurology, London, UK

[5]Kings College London, London, UK

[6]Clinical Board Medicine (Neuroscience), Barts Health NHS Trust, The Royal London Hospital, London, UK

*Klaus Schmierer and Tobias C Wood contributed equally to this work

Address correspondence to: Amy McDowell

E mail: a.mcdowell@ucl.ac.uk

Type of manuscript: Article

Running Title: Quantitative MR of MS Spinal Cord

Word Count: 2594

Acknowledgements

We thank F. Scaravilli for expert support in reviewing and reporting cases used in this study; and R. Reynolds, D. Gveric, and the team of the Multiple Sclerosis and Parkinson's Disease Tissue Bank based at Imperial College, London, for supplying the tissue.

Conflicts of Interest

GJB received honoraria for teaching from GE Healthcare at the time of this study. There are no other known conflicts of interest to disclose

Ethics:

This study was covered by the UK Multiple Sclerosis Tissue Bank approval (Research Ethics Committee reference number 08/MRE09/31).

Funding

This study was supported by Barts Charity (grant code # 468/1506). DLT is supported by the UCL Leonard Wolfson Experimental Neurology Centre (PR/ylr/18575), the Wellcome Trust (Centre award 539208) and the UCLH NIHR Biomedical Research Centre.

Authorship

All authors have made substantial contributions to 1) conception and design, or acquisition of data, or analysis and interpretation of data; 2) drafting the article or revising it critically for important intellectual content; and 3) final approval of the version to be published.

Abstract

Purpose: Validation of quantitative MR measures for myelin imaging in the post mortem Multiple Sclerosis (MS) spinal cord.

Methods: Four fixed spinal cord samples were imaged first with a 3T clinical MR scanner to identify areas of interest for scanning, and then with a 7T small bore scanner using a multicomponent driven equilibrium single pulse observation of T1 and T2 protocol to produce apparent proton density (aPD), T1, T2, myelin water, intra-cellular water and free water fraction maps. After imaging, the cords were sectioned and stained with histological markers (Haematoxylin & Eosin, Myelin Basic Protein and neurofilament protein), which were quantitatively compared to the MR maps.

Results: Excellent correspondence was found between high resolution MR parameter maps and histology, particularly for aPD MRI and Myelin Basic Protein staining.

Conclusion: High resolution quantitative MR imaging of the spinal cord provides biologically meaningful measures, and could be beneficial to diagnose and track MS lesions in the spinal cord.

Keywords: myelin water fraction, spinal cord, multiple sclerosis

Introduction

The myelin sheath is an extended and modified plasma membrane wrapped around axons in a spiral fashion[1]. Myelin is composed of about 40% water, whilst the dry mass consist of about 80% lipids, mainly the glycolipid galactocerebroside, and 20% protein[2]. Due to its importance for normal function of the nervous system, and severe consequences of myelin damage in demyelinating diseases, such as multiple sclerosis (MS), the non-invasive in vivo assessment of myelin remains a key focus of imaging research, not least in the era of regenerative medicine[3].

The spinal cord is most commonly affected in people with MS (pwMS) at presentation[4,5]. Lesions in the spinal cord have been shown to predict both a diagnosis of MS in patients with radiologically isolated, as well as clinically isolated, syndromes of demyelination (RIS, CIS)[6,7]; they are also associated with more severe disability[6,8]. As MS evolves over time, much of the permanent and deteriorating disability in people with MS affects lower body functions, including lack of sphincter control, sexual dysfunction, and impaired leg movement and coordination, resembling the clinical syndrome of progressive myelopathy[9-12]. Metrics such as spinal cord cross-sectional area (CSA) have been shown to be associated with MS- related disability in vivo[13]. However, CSA is affected by numerous elements of MS pathology including inflammation, edema, myelin content, the number of axons and gliosis.

MRI is widely used in the assessment of MS, but standard qualitative T1- and T2-weighted images are largely non-specific for the underlying pathology[14]. Quantitative MRI (qMRI) has the potential to distinguish specific tissue features, such as separating

demyelination from axonal loss[15]. Multi-Component relaxometry is a family of methods that can quantify the fractional amount of water in different tissue environments by exploiting the differences in relaxation time values. In the nervous system, these environments include free water in cerebrospinal fluid (CSF), intra- and extra-cellular water (IEW) and, most importantly in the context of demyelinating diseases, water 'trapped' between the myelin bilayers. The ratio of myelin water signal to total water signal is termed myelin water fraction (MWF)[16].

Along with other related quantitative measures, including the relaxation times themselves, MWF has shown promise to identify specific features of MS pathology and monitoring disease progression[17,18]. The gold-standard method for evaluating the MWF is analysis of a Multi-Echo T2 (MET2) relaxation curve[16]. The MET2 method has been previously compared to histology in *post mortem* brain at 1.5T[19], and Laule and coworkers demonstrated strong correlation of MWF in MS tissue samples at 7T with luxol fast blue (LFB) staining intensity for myelin on histology[20]. These studies support the hypothesis that myelin can be mapped in the brain using MWF. However, clinical translation of MET2 has been hampered by the long acquisition time required[21].

In contrast, gradient echo based methods, such as the Driven Equilibrium Single-Pulse Observation of T1 & T2 (DESPOT1&2), are inherently fast[22]. A multi-component version (mcDESPOT) has been used in clinical studies of MS[23], primary lateral sclerosis[24] and monitoring myelin development in children[25-29]. However, histological validation has been lacking, and recent work has shown that mcDESPOT suffers from unpredictable bias but as there was sufficient data for analysis we present it here[30,31].

Given significant efforts in MS research are directed towards development of strategies for myelin repair (remyelination)[32], imaging biomarkers of myelin are desirable. To establish whether mcDESPOT could provide such an index (or indices) we undertook correlative experiments using post mortem spinal cord, to quantitatively compare MRI and histology data.

Methods

Formalin-fixed spinal cords were placed on a Perspex frame and inserted into glass tubes. The formalin was drained and the tubes then filled with perfluoropolyether (Fomblin, Solvay Solutions UK Ltd) to provide a susceptibility-matched signal-free background (Supporting Information Figure S1).

Qualitative structural MRI was performed on the whole cords at 3T (Achieva Tx, Philips Healthcare, Best, Netherlands) using a 15 element SENSE Spine coil and a Turbo Spin Echo (TSE) sequence with the following parameters: echo time (TE) 16ms, repetition time (TR) 5000ms, voxel size 0.4x0.4x2.0mm^3). Nine areas of interest were identified by a neurologist with >20 years of experience in reading MRI of pwMS (KS) for scanning at 7T. The thoracic level 1 was marked with a radiologically opaque marker tied to the nerve root; measurements of distance from the marker for each lesion were noted and used to inform positioning of the glass tube for subsequent 7T scanning.

Next, the cords were scanned using a 7T pre-clinical scanner (Agilent Technologies, Santa Clara, California, USA) and 39-mm diameter quadrature transmit-receive RF coil (Rapid Biomedical GmbH, Rimpar, Germany) designed for whole-body rodent imaging. As the human spine is longer than the achievable field-of-view (FOV) with this setup, for each area of interest the glass tubes were moved in or out of the RF coil as required to place the desired area at both the centre of the RF coil and the isocentre of the magnet. We observed that the active area of the RF coil was longer than the linear region of the image encoding gradients. As the samples were long enough to protrude

into this region, protons that were excited by the RF but not encoded by the gradients resulted in a "zipper artefact" in some images. This was minimised by careful rotation of the samples so that the artefacts did not intrude into areas required for analysis. In most samples a small quantity of formalin remained after draining which produced bright signal at the top of the sample tube. To avoid this wrapping into the tissue the FoV was increased in the vertical direction.

Spoiled gradient echo (SPGR) and balanced steady-state free precession (bSSFP) (with 2 RF phase-cycles) sequences were acquired with the parameters given in Table 1, along with an Actual Flip Angle (AFI) acquisition for B_1 correction[33]. Images were resampled to 150x150x300µm^3 for processing. The images were processed using the open-source Quantitative Imaging Tools (QUIT) C++ toolbox[34] (available from http://github.com/spinicist/QUIT). T1 maps were generated using non-linear least squares fitting to images with all flip angles[35,36], and T2 and apparent Proton Density (aPD) maps were generated using the DESPOT2-FM method[37].

Calculation of MWF from mcDESPOT requires the a-priori specification of valid initial ranges of T1 and T2 for each water component[30,38]. It has been recognized that in post-mortem tissue these relaxation times change following fixation[39-41]. The single-component T1 and T2 of white matter in a healthy cord was used as a reference point for the myelin water T1 and T2, healthy grey matter relaxation times were used as reference points for the intra-/extra-cellular water T1 and T2, and literature values were used for the free-water fraction[38]. Fitting parameters including the ranges used for each water component are shown in Table 2. Non-overlapping ranges that

encompassed the reference points or literature values for these parameters were used. It has been shown that neglecting the effect of TE in the SPGR and bSSFP signal models lead to large errors in derived MWF values, so the echo-time corrected signal model was used[42].

MR parameter maps were then matched with histology using positional information (cord level and distance of the lesion from the marker) from the 3T whole cord scans, and checked against anatomical features (such as lesion shape and grey matter anatomy) in the histology and 7T images. MIPAV (http://mipav.cit.nih.gov/) was used to manually define ROIs on aPD maps and transfer them to all other maps for ROI analysis.

For histology, cords were dissected axially into blocks of 5mm thickness. Each tissue block was then marked with tissue dye to retain information on its spatial orientation and processed for embedding in paraffin. 10μm thick sections were cut from each tissue block using a Shandon Finesse ME1 microtome (Thermo-Scientific, UK. Care was taken to cut the sections in a plane perpendicular to the anterior spinal artery. The sections were mounted on Superfrost1 slides (VWR, UK) and left in a 608C oven overnight.

Serial sections of each block were stained for haematoxylin and eosin (H&E), phosphorylated neurofilaments (SMI-31, mouse monoclonal, 1:1000, Abcam, UK) and myelin basic protein (MBP, SMI-94, mouse monoclonal, 1:100, Covance, Princeton, NJ, USA) following a modified protocol [43-45].

Focal areas of complete myelin loss were identified on MBP immuno-stained sections as demyelinated lesions in the white (WML) and grey matter (GML). Cellularity and axonal counts were determined by counting the number of cells in four square ROIs (size: 120×120μm^2) cast randomly onto WML and non-lesional white matter (NLWM) on H&E and SMI-31 stained sections respectively (Supporting Information Figure S2). Cellularity and axonal counts were expressed as cells/mm^2 and axons/mm^2 respectively. Unpaired two-tailed t-tests were performed to compare MWF, IEWF and FWF values in the NLWM and WML ROIs.

Results

Formalin-fixed spinal cords of three pwMS (one male, two female), and one male control subject with no neurological disease were used. The MS cords were from donors who died at the age of 67-87 years. Their disease duration had been 8-44 years. The MS cords had been fixed for 1127-1441 days. The control subject died aged 89 years. Duration of fixation of this cord was 1366 days.

Figure 1 shows matched histology and quantitative MR parameter maps of spinal cords from the three MS patients and one control subject. Excellent visual correspondence was observed between the anatomic detail on histology images and aPD maps. Both T1 and T2 maps showed less contrast between lesion and healthy tissue than aPD, while the MWF produced high contrast, matching well with the myelin histology in the cords from pwMS. The IEWF map showed, as expected, the inverse of the MWF map (lower in myelinated areas and higher elsewhere). Surprisingly, the FWF map was non-zero in healthy tissue area especially in the control cords but decreased to zero in lesion areas. Cord MS454 had no grey matter areas that could definitely be determined as normal appearing grey matter. MBP staining, aPD, MWF, IEWF, and FWF images only are shown together in Supporting Information Figure S3 to facilitate comparison of the maps.

Quantitative histology results and mean values of the MR parameters from the ROIs are given in Table 3. Cellularity and axon count and MBP staining fraction were reduced in lesions compared to normal white-matter; MWF also showed a decrease in lesion areas, while the IEWF increased. We observed a noticeable decrease in the FWF fraction. It should be noted that the MBP staining fraction can only be compared

within a single batch, and hence there is variable staining between the pathological cords and the control cord, which was stained at a later date. Therefore, the MBP values were not entered into the correlation analysis for the control cord.

Graphs of the MWF, IEWF and FWF values in the NLWM, NLGM and WM and GM lesion are shown in Supporting Information Figure S4. MWF, IEWF and FWF were all significantly different between NLWM and WML ($P < 0.0001$). Graphs of correlation (Pearson's correlation) between histological and MR indices over all white matter lesions and non-lesional white matter in MS cords, and control white matter in control cords (axon counts vs. aPD, T1, MWF, and MBP stain vs. T1, MWF) are shown in Figure 2. All are significant (Pearson's R and P-values shown on graphs and tabled in Supporting Information Table S1). Correlations between MWF and aPD in individual white matter types (WML, NLWM and control WM) and histological indices are shown in Supporting Information Figure S5 and S6 respectively. Correlation between both cell nuclei and axon counts and MWF in WML were not significant. Correlation between nuclei counts and MWF in NLWM and control WM was just significant ($P=0.046$), but not significant between axons and MWF in NLWM and control WM. This significance is likely due to the difference in nuclei between control data and NLWM rather than a correlation with MWF.

Discussion

Our results show that with high resolution scanning at 7T, good correspondence between qMRI and histological metrics is observed. aPD maps show excellent contrast between healthy and pathological tissue, and T1 & T2 maps provide quantitative measures that correlate with quantitative histology measures.

The myelin water fraction (MWF) maps show clear differentiation between lesion and non-lesional tissue. The non-zero FWF in the healthy control cord is an unexpected finding, as fixed tissue has not been thought to contain water protons with a long T2. This may indicate infiltration by the fixative or may simply be due to bias in the fitting procedure[31]. The FWF component in the control cords displays better contrast between WM and GM than the MWF for instance, which could be caused by either of these mechanisms. The measured FWF is lower in lesions in pathological cords, which may also be due to said bias or could indicate the assumption that the FWF is non-exchanging, i.e. that water cannot move between the FWF and IE-water pools, is invalid. In lesions it is possible that biological barriers between these pools break down such that they behave as one, with a common T1 and T2.

Our samples were not rinsed of fixative before acquisition as this could cause degradation of the tissue, and therefore contained formaldehyde. Formaldehyde causes known shortening of the T1 and T2 values reducing the differences between the myelin and intra-/extra-cellular compartments[46]. The stochastic region contraction (SRC) search algorithm used in mcDESPOT may not be able to consistently differentiate the signal from the different water pools in this situation. Care was taken

to choose appropriate fitting ranges (see Table 2), but derived MWF values are highly dependent on the selected parameter ranges, especially when the SRC algorithm is used for fitting[31,47]. An alternate approach such as the Bayesian priors of Bouhrara et al. may improve fitting accuracy[48]. Unfixed tissue is challenging to scan in a suitable time frame after death in humans and may show decomposition over a long scan time but, if possible, further validation in unfixed tissue would be desirable as the water pools should exhibit similar separation as in-vivo tissue.

The IEWF maps also show good definition between tissue types, with high values in lesional tissue. This implies more space in larger cells and between the cells in these areas. This has been postulated previously by Christiansen et al.[49], who found the apparent diffusion coefficient increased in MS lesions and suggested that this may be related to an increase in the extracellular space due to oedema and demyelination. They hypothesised the myelin removed is replaced by water resulting in an increase of the extracellular space and thereby the formerly restricted diffusion becomes less restricted.

Despite the issues related to fitting the mcDESPOT model, the MWF and IEWF showed good contrast and anatomic correspondence to the histology images, while the single component T1 and T2 maps showed comparatively low contrast. However, the aPD maps also show excellent correspondence with histology, with increased values in lesion areas. It should be noted that the because MWF and IEWF are defined as fractions, the aPD is effectively removed from the mcDESPOT measures; hence, the contrast in the aPD maps is orthogonal information to that in the mcDESPOT

parameter maps. Our results imply that if, for example, only the MWF is considered then an important additional source of information, namely the total water content in a voxel, will be missed.

Conclusion

High resolution quantitative MR parameter maps offer an alternative modality to histology for ex vivo quantitative assessment of MS spinal cord lesions. MWF maps showed good contrast between lesional and non-lesional tissue. Proton density, which reflects total water content, correlated significantly in MS lesions and offers additional information compared to the mcDESPOT parameter maps. The mcDESPOT model may benefit from the use of a Bayesian priors algorithm for more challenging conditions.

Table Captions

Table 1

MRI sequence acquisition parameters

Table 2

The minimum and maximum values that were set for T1 and T2 of each component during mcDESPOT fitting. The expected T1 and T2 of myelin and intra-/extra-cellular water were set significantly lower than for an equivalent in-vivo experiment because of formalin fixation is known to shorten these values. Fraction constraints constrain the MWF and FWF to within expected values to prevent convergence to an erroneous local minima. Myelin residence time is the mean time a water molecule stays in the myelin pool before exchanging to the IE-pool.

SPGR = Spoiled Gradient echo; bSSFP = Steady-State Free Precession; AFI = Actual Flip Angle

Table 3

Histology and MR indices for each region of interest. There are no lesions in the control cords. Hence, these entries are marked not applicable (NA). All three histology measures were reduced in lesions compared to normal white-matter. WML= white matter lesion; NLWM= non-lesional white matter.

MWF = Myelin Water Fraction; IEWF = Intra/Extra- cellular Water Fraction; FWF = Free Water Fraction

Table 1

Sequence	TE/TR [ms]	Flip-Angles	Voxel Size [μm^3]	Matrix Size
SPGR	11.3/25	6, 8, 10, 15, 20, 25, 35, 45	100x125x200	160x160x160
bSSFP	2/4	14, 17, 20, 25, 35, 50, 65	100x125x200	160x160x160
AFI	2.62/7.5	55	250x250x500	64x64x64

Table 2

	MWF	IEW	FWF
T1 [ms]	50-350	400-800	1000-5000
T2 [ms]	8-14	14-25	200-1500
Fraction constraints [%]	0.1-50	NA	0.1-99
Myelin residence time [ms]	10 – 250	NA	NA

Table 3

Sample	MBP Stain %		Nuclei/mm²		Axons/mm²		APD (Arb Units)		T1 [ms]		T2 [ms]		MWF %		IEF %		FWF %	
	WML	NLWM	WML	NLWM	WML	NLWM	WML	NLWM	WML	NLWM	WML	NLWM	WML	NLWM	WML	NLWM	WML	NLWM
MS1 C8	1.78	83.92	1736	1858	7969	20174	6.0E+05	4.5E+05	708.3	445.3	21.4	16	3.6	18.5	96.2	80.4	0.2	1.2
MS1 T3	5.17	78.56	1458	2546	8767	14601	4.9E+05	3.4E+05	518.9	390.6	17.4	14.7	14.1	28.1	85.3	69.7	0.6	2.3
MS1 T5	3.35	87.86	1892	1944	2326	11782	6.1E+05	4.1E+05	604.3	407.2	19.8	15.4	8.7	23.3	91	74.4	0.3	2.3
MS1 T11	1.9	88.31	2760	2778	9514	15122	5.8E+05	4.2E+05	590.9	394.9	19.5	15.2	9	24.9	90.8	76.7	0.2	4.8
MS2 T11	2.89	63.4	2170	2135	7934	12604	5.6E+05	4.2E+05	578.2	517.4	17.4	17.5	13	14.8	86	83	1	2.2
MS3 C07A	15.71	61.46	1215	1615	8281	18843	5.4E+05	4.2E+05	663.6	449.7	18.4	15.4	5.5	23	93.8	75.7	0.7	1.3
MS3 C07B	0.59	43.39	1233	1389	7639	15625	5.1E+05	5.0E+05	634.7	478.9	19.1	15.5	7	18.2	92.6	79.8	0.4	2
Control C7	NA	73.91	NA	27018	NA	15634	NA	4.5E+05	NA	403.5	NA	13.9	NA	29.8	NA	67.1	NA	3.1
Control T8	NA	44.47	NA	27456	NA	16571	NA	4.4E+05	NA	410.4	NA	14.3	NA	29.1	NA	68.5	NA	2.5

Figure captions

Figure 1

Histology and MR maps of three MS spinal cords, from top to bottom, sections taken from spinal cord 1 at levels C8, T3, T5 and T11, spinal cord 2 at T11 and spinal cord 3, two lesions at C7. Control cord sections at C8 and T9 are shown on the bottom two rows. The histological slides stained with MBP, H&E and SMI at the level of each lesion found are shown next to aPD, T1, T2, MWF, IEF and FWF maps at the same level. From left to right: MBP, H&E, SMI stained sections, aPD, T1, T2, MWF, IEWF and FWF. All images were scaled between identical limits for each contrast so a comparison could be made (aPD 0 - 5.0x10^5 PU; T1 0 - 800 ms; T2 10 - 20 ms; MWF 0 - 0.5 %; IEWF 0 - 1 %; FWF 0 - 0.05 %) MWF = Myelin Water Fraction; IEWF = Intra/Extra- cellular Water Fraction; FWF = Free Water Fraction

Figure 2

Correlation between histological and MR indices over all white matter lesion, and non-lesional white matter in MS cords and control white matter in control cords. Correlation of axons against aPD, T1 and myelin water fraction (A, B and C respectively) and MBP against aPD and T1 (D and E respectively). Control cord white matter data is shown by the red data points, non-lesional white matter by black dots, and lesional white matter by green dots. The best fit line is shown with 95% confidence intervals. R = Person's R value and P = P-value

Figures

Figure 1

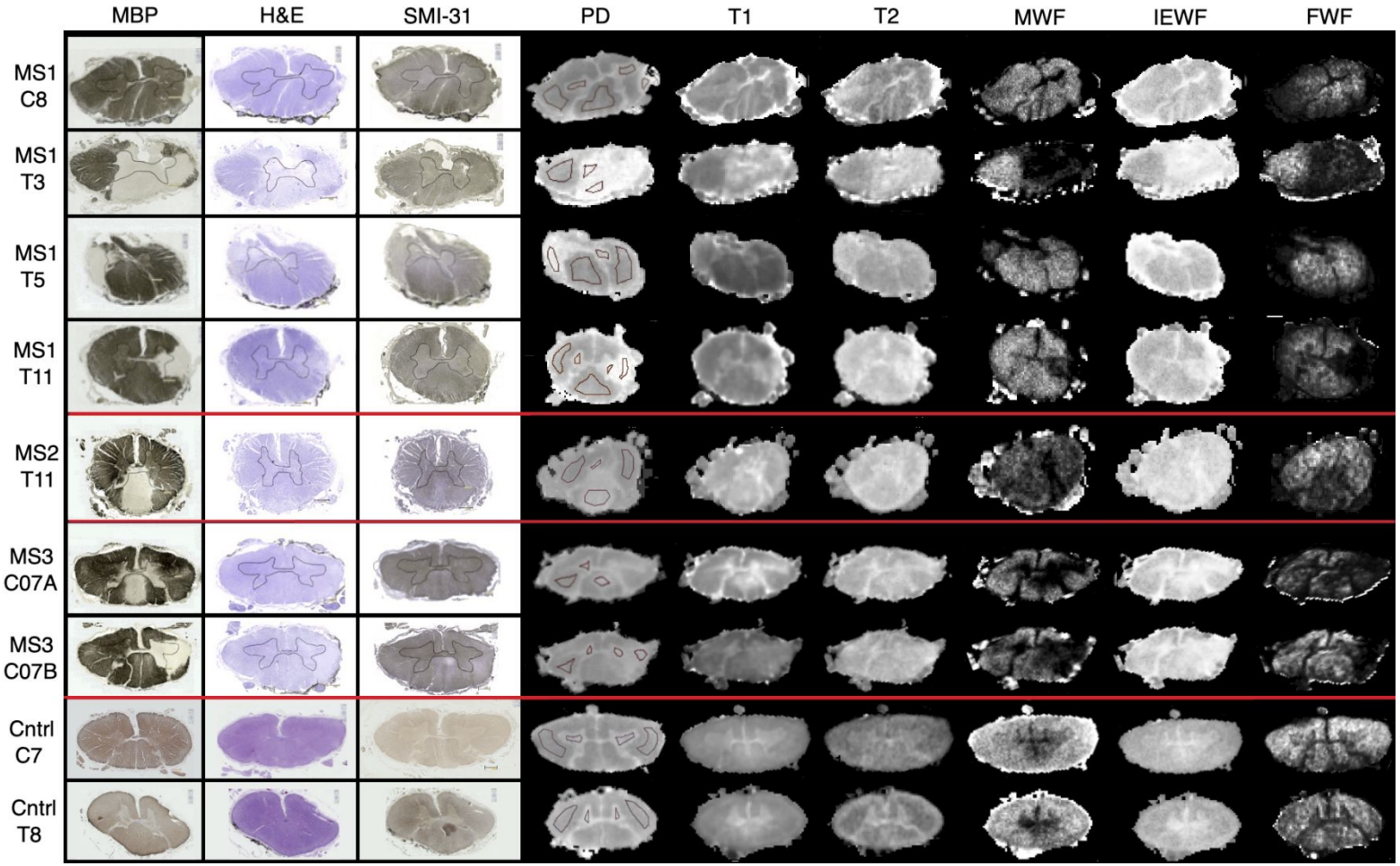

Figure 2

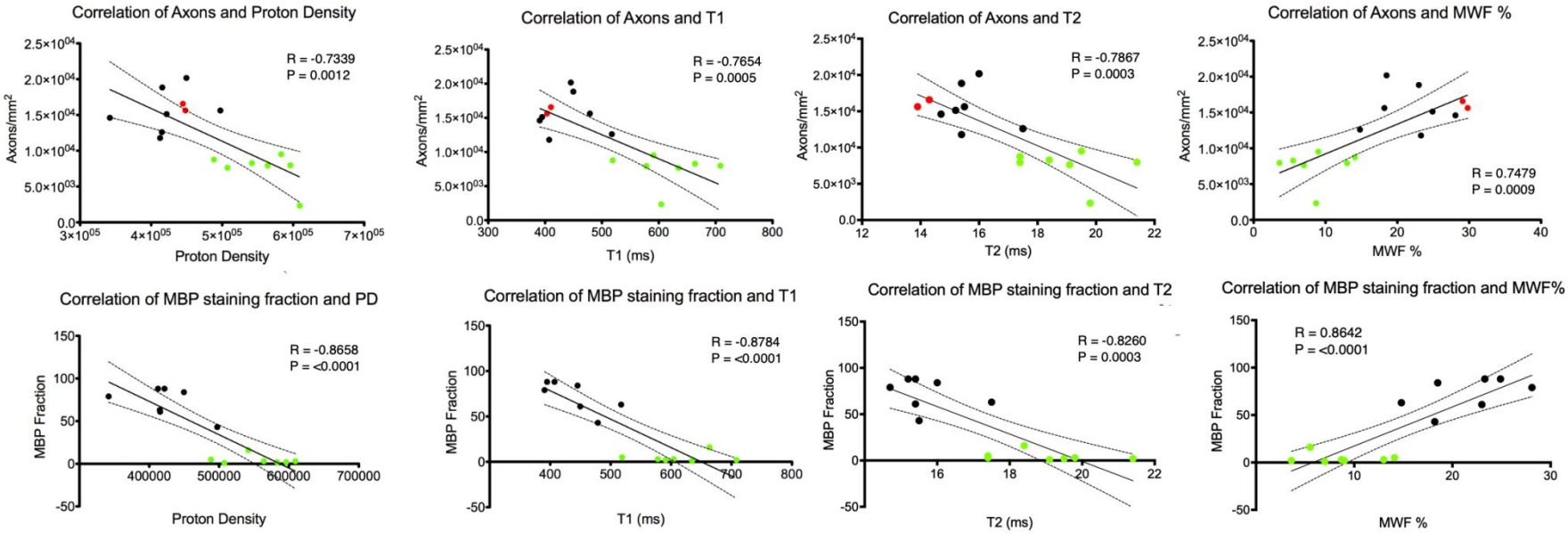
Correlation of Axons and Proton Density
R = -0.7339
P = 0.0012
Axons/mm2
Proton Density
Correlation of Axons and T1
R = -0.7654
P = 0.0005
Axons/mm2
T1 (ms)
Correlation of Axons and T2
R = -0.7867
P = 0.0003
Axons/mm2
T2 (ms)
Correlation of Axons and MWF %
R = 0.7479
P = 0.0009
Axons/mm2
MWF %
Correlation of MBP staining fraction and PD
R = -0.8658
P = <0.0001
MBP Fraction
Proton Density
Correlation of MBP staining fraction and T1
R = -0.8784
P = <0.0001
MBP Fraction
T1 (ms)
Correlation of MBP staining fraction and T2
R = -0.8260
P = 0.0003
MBP Fraction
T2 (ms)
Correlation of MBP staining fraction and MWF%
R = 0.8642
P = <0.0001
MBP Fraction
MWF %

References

1. Raine CS. Morphology of Myelin and Myelination. In: Morell P, ed. *Myelin.* Boston, MA: Springer US; 1984:1-50.
2. Morell P, Quarles RH. The Myelin Sheath. In: Siegel GJ, Agranoff BW, Albers RW, eds. *Basic Neurochemistry: Molecular, Cellular and Medical Aspects.* Philadelphia: Lippincott-Raven; 1999.
3. Neumann B, Foerster S, Zhao C, et al. Problems and Pitfalls of Identifying Remyelination in Multiple Sclerosis. *Cell Stem Cell.* 2020;26(5):617-619.
4. Katz Sand I. Classification, diagnosis, and differential diagnosis of multiple sclerosis. *Current opinion in neurology.* 2015;28(3):193-205.
5. Mowry EM, Pesic M, Grimes B, Deen S, Bacchetti P, Waubant E. Demyelinating events in early multiple sclerosis have inherent severity and recovery. *Neurology.* 2009;72(7):602-608.
6. Arrambide G, Rovira A, Sastre-Garriga J, et al. Spinal cord lesions: A modest contributor to diagnosis in clinically isolated syndromes but a relevant prognostic factor. *Multiple sclerosis (Houndmills, Basingstoke, England).* 2018;24(3):301-312.
7. Okuda DT, Mowry EM, Cree BAC, et al. Asymptomatic spinal cord lesions predict disease progression in radiologically isolated syndrome. *Neurology.* 2011;76(8):686.
8. Brownlee WJ, Altmann DR, Alves Da Mota P, et al. Association of asymptomatic spinal cord lesions and atrophy with disability 5 years after a clinically isolated syndrome. *Multiple sclerosis (Houndmills, Basingstoke, England).* 2017;23(5):665-674.
9. Giovannoni G, Cutter G, Sormani MP, et al. Is multiple sclerosis a length-dependent central axonopathy? The case for therapeutic lag and the asynchronous progressive MS hypotheses. *Mult Scler Relat Disord.* 2017;12:70-78.
10. Kearney H, Miller DH, Ciccarelli O. Spinal cord MRI in multiple sclerosis--diagnostic, prognostic and clinical value. *Nature reviews Neurology.* 2015;11(6):327-338.
11. Kremenchutzky M, Rice GP, Baskerville J, Wingerchuk DM, Ebers GC. The natural history of multiple sclerosis: a geographically based study 9: observations on the progressive phase of the disease. *Brain : a journal of neurology.* 2006;129(Pt 3):584-594.
12. McDonald I, Compston A. Chapter 6 - The symptoms and signs of multiple sclerosis. In: Compston A, Confavreux C, Lassmann H, et al., eds. *McAlpine's Multiple Sclerosis (Fourth Edition).* Edinburgh: Churchill Livingstone; 2006:287-346.
13. Losseff NA, Webb SL, O'Riordan JI, et al. Spinal cord atrophy and disability in multiple sclerosis. A new reproducible and sensitive MRI method with potential to monitor disease progression. *Brain : a journal of neurology.* 1996;119 (Pt 3):701-708.
14. Giorgio A, De Stefano N. Effective Utilization of MRI in the Diagnosis and Management of Multiple Sclerosis. *Neurologic clinics.* 2018;36(1):27-34.

15. Schmierer K, McDowell A, Petrova N, Carassiti D, Thomas DL, Miquel ME. Quantifying multiple sclerosis pathology in post mortem spinal cord using MRI. *NeuroImage.* 2018;182:251-258.
16. MacKay A, Whittall K, Adler J, Li D, Paty D, Graeb D. In vivo visualization of myelin water in brain by magnetic resonance. *Magnetic resonance in medicine.* 1994;31(6):673-677.
17. Vavasour IM, Laule C, Li DK, et al. Longitudinal changes in myelin water fraction in two MS patients with active disease. *Journal of the neurological sciences.* 2009;276(1-2):49-53.
18. MacKay AL, Vavasour IM, Rauscher A, et al. MR relaxation in multiple sclerosis. *Neuroimaging clinics of North America.* 2009;19(1):1-26.
19. Moore GR, Leung E, MacKay AL, et al. A pathology-MRI study of the short-T2 component in formalin-fixed multiple sclerosis brain. *Neurology.* 2000;55(10):1506-1510.
20. Laule C, Kozlowski P, Leung E, Li DK, Mackay AL, Moore GR. Myelin water imaging of multiple sclerosis at 7 T: correlations with histopathology. *NeuroImage.* 2008;40(4):1575-1580.
21. Ljungberg E, Vavasour I, Tam R, et al. Rapid myelin water imaging in human cervical spinal cord. *Magnetic resonance in medicine.* 2017;78(4):1482-1487.
22. Deoni SC, Rutt BK, Arun T, Pierpaoli C, Jones DK. Gleaning multicomponent T1 and T2 information from steady-state imaging data. *Magnetic resonance in medicine.* 2008;60(6):1372-1387.
23. Kitzler HH, Su J, Zeineh M, et al. Deficient MWF mapping in multiple sclerosis using 3D whole-brain multi-component relaxation MRI. *NeuroImage.* 2012;59(3):2670-2677.
24. Kolind S, Sharma R, Knight S, Johansen-Berg H, Talbot K, Turner MR. Myelin imaging in amyotrophic and primary lateral sclerosis. *Amyotrophic lateral sclerosis & frontotemporal degeneration.* 2013;14(7-8):562-573.
25. Deoni SC, Dean DC, 3rd, O'Muircheartaigh J, Dirks H, Jerskey BA. Investigating white matter development in infancy and early childhood using myelin water faction and relaxation time mapping. *NeuroImage.* 2012;63(3):1038-1053.
26. Deoni SC, Dean DC, 3rd, Piryatinsky I, et al. Breastfeeding and early white matter development: A cross-sectional study. *NeuroImage.* 2013;82:77-86.
27. Spader HS, Ellermeier A, O'Muircheartaigh J, et al. Advances in myelin imaging with potential clinical application to pediatric imaging. *Neurosurgical focus.* 2013;34(4):E9.
28. Miele A, Pan J, Walker L, et al. B-74The Relationship of Myelin Content and Measures of Executive Functioning in Typically Developing Children. *Archives of clinical neuropsychology : the official journal of the National Academy of Neuropsychologists.* 2014;29(6):564.
29. Miele A, Pan J, Walker L, et al. B-75Neural Correlates of Emerging Executive Functioning in 2-5 Year Olds. *Archives of clinical neuropsychology : the official journal of the National Academy of Neuropsychologists.* 2014;29(6):565.
30. Lankford CL, Does MD. On the inherent precision of mcDESPOT. *Magnetic resonance in medicine.* 2013;69(1):127-136.

31. West DJ, Teixeira R, Wood TC, Hajnal JV, Tournier JD, Malik SJ. Inherent and unpredictable bias in multi-component DESPOT myelin water fraction estimation. *NeuroImage.* 2019;195:78-88.
32. Cunniffe N, Coles A. Promoting remyelination in multiple sclerosis. *Journal of neurology.* 2021;268(1):30-44.
33. Yarnykh VL. Actual flip-angle imaging in the pulsed steady state: a method for rapid three-dimensional mapping of the transmitted radiofrequency field. *Magnetic resonance in medicine.* 2007;57(1):192-200.
34. Wood TC, Simmons C, Hurley SA, et al. Whole-brain ex-vivo quantitative MRI of the cuprizone mouse model. *PeerJ.* 2016;4:e2632.
35. Chang LC, Koay CG, Basser PJ, Pierpaoli C. Linear least-squares method for unbiased estimation of T1 from SPGR signals. *Magnetic resonance in medicine.* 2008;60(2):496-501.
36. Stikov N, Boudreau M, Levesque IR, Tardif CL, Barral JK, Pike GB. On the accuracy of T mapping: Searching for common ground. *Magnetic resonance in medicine.* 2014.
37. Deoni SC. Transverse relaxation time (T2) mapping in the brain with off-resonance correction using phase-cycled steady-state free precession imaging. *Journal of magnetic resonance imaging : JMRI.* 2009;30(2):411-417.
38. Deoni SC, Matthews L, Kolind SH. One component? Two components? Three? The effect of including a nonexchanging "free" water component in multicomponent driven equilibrium single pulse observation of T1 and T2. *Magnetic resonance in medicine.* 2013;70(1):147-154.
39. Tovi M, Ericsson A. Measurements of T1 and T2 over time in formalin-fixed human whole-brain specimens. *Acta radiologica (Stockholm, Sweden : 1987).* 1992;33(5):400-404.
40. Blamire AM, Rowe JG, Styles P, McDonald B. Optimising imaging parameters for post mortem MR imaging of the human brain. *Acta radiologica (Stockholm, Sweden : 1987).* 1999;40(6):593-597.
41. Schmierer K, Wheeler-Kingshott CA, Tozer DJ, et al. Quantitative magnetic resonance of postmortem multiple sclerosis brain before and after fixation. *Magnetic resonance in medicine.* 2008;59(2):268-277.
42. Bouhrara M, Spencer RG. Incorporation of nonzero echo times in the SPGR and bSSFP signal models used in mcDESPOT. *Magnetic resonance in medicine.* 2015;74(5):1227-1235.
43. Geurts JJ, Bo L, Pouwels PJ, Castelijns JA, Polman CH, Barkhof F. Cortical lesions in multiple sclerosis: combined postmortem MR imaging and histopathology. *AJNR American journal of neuroradiology.* 2005;26(3):572-577.
44. Tallantyre EC, Bo L, Al-Rawashdeh O, et al. Clinico-pathological evidence that axonal loss underlies disability in progressive multiple sclerosis. *Multiple sclerosis (Houndmills, Basingstoke, England).* 2010;16(4):406-411.
45. Petrova N, Carassiti D, Altmann DR, Baker D, Schmierer K. Axonal loss in the multiple sclerosis spinal cord revisited. *Brain pathology (Zurich, Switzerland).* 2018;28(3):334-348.
46. Seifert AC, Umphlett M, Hefti M, Fowkes M, Xu J. Formalin tissue fixation biases myelin-sensitive MRI. *Magnetic resonance in medicine.* 2019;82(4):1504-1517.

47. Bouhrara M, Reiter DA, Celik H, Fishbein KW, Kijowski R, Spencer RG. Analysis of mcDESPOT- and CPMG-derived parameter estimates for two-component nonexchanging systems. *Magnetic resonance in medicine.* 2016;75(6):2406-2420.
48. Bouhrara M, Spencer RG. Improved determination of the myelin water fraction in human brain using magnetic resonance imaging through Bayesian analysis of mcDESPOT. *NeuroImage.* 2015.
49. Christiansen P, Gideon P, Thomsen C, Stubgaard M, Henriksen O, Larsson HB. Increased water self-diffusion in chronic plaques and in apparently normal white matter in patients with multiple sclerosis. *Acta neurologica Scandinavica.* 1993;87(3):195-199.

Supporting Information

Supporting Information Figure S1 Caption

Whole spinal cord secured in a glass tube and immersed in perfluoropolyether ready for scanning.

Supporting Information Figure S2 Caption

Example H&E stained section (left, A) with four square ROIs positioned in the red outlined region (top right, B), grey matter is outlined in black. Zoomed section (bottom right, C) shows detail in square ROI. Cellularity and axonal counts were determined by counting the number of cells in four square ROIs (size: 120×120μm^2) cast onto lesional and non-lesional white matter on the H&E and SMI-31 stained sections.

Supporting Information Figure S3 Caption

Expanded Figure taken from Figure 2 showing only MDP, PD, MWF, IEWF and FWF to facilitate comparison

Supporting Information Figure S4 Caption

Box and whisker plots of all MR parameters in each tissue type. Red points are control samples, for which there is no lesional data. Differences in all parameters were present between NLWM and WM lesion. Centre line is the mean with whiskers of one standard deviation.

Supporting Information Table S1 Caption

Correlation coefficients for graphs shown in Figure 2

Supporting Information Figure S5 Caption

Graphs of correlation for myelin water fraction separated into individual white matter types expanded from Figure 2; white matter lesion and non-lesional white matter. Correlations with nuclei against myelin water fraction in white matter lesion and non-lesional white matter in MS cords and control white matter in control cords (A and C respectively) and axons against myelin water fraction in white matter lesion and non-lesional white matter in MS cords and control white matter in control cords (B and D respectively). Control cord white matter data is shown by the red data points. The best fit line is shown with the 95% confidence intervals.

Supporting Information Figure S6 Caption

Graphs of correlation for proton density separated into individual white matter types expanded from Figure 2; white matter lesion and non-lesional white matter. Correlations with nuclei against proton density in white matter lesion and non-lesional white matter in MS cords and control white matter in control cords (A and C respectively) and axons against proton density in white matter lesion and non-lesional white matter in MS cords and control white matter in control cords (B and D respectively). Control cord white matter data is shown by the red data points. The best fit line is shown with the 95% confidence intervals.

High Resolution Quantitative MRI of Multiple Sclerosis Spinal Cord Lesions

Amy R McDowell[1], Natalia Petrova[2], Daniele Carassiti[2], Marc E Miquel[3], David L Thomas[4], Gareth J Barker[5], Klaus Schmierer*[2,6], Tobias C Wood*[5]

Affiliations:

[1]Queen Square Centre for Neuromuscular Diseases, UCL, London, UK

[2]The Blizard Institute (Neuroscience, Surgery & Trauma), Queen Mary University of London, Barts and The London School of Medicine & Dentistry, London, UK

[3]Clinical Physics, Barts Health NHS Trust

[4]Department of Brain Repair and Rehabilitation, UCL Queen Square Institute of Neurology, London, UK

[5]Kings College London, London, UK

[6]Clinical Board Medicine (Neuroscience), Barts Health NHS Trust, The Royal London Hospital, London, UK

*Klaus Schmierer and Tobias C Wood contributed equally to this work

Address correspondence to: Amy McDowell

E mail: a.mcdowell@ucl.ac.uk

Type of manuscript: Article

Running Title: Quantitative MR of MS Spinal Cord

Word Count: 2594

Acknowledgements

We thank F. Scaravilli for expert support in reviewing and reporting cases used in this study; and R. Reynolds, D. Gveric, and the team of the Multiple Sclerosis and Parkinson's Disease Tissue Bank based at Imperial College, London, for supplying the tissue.

Conflicts of Interest

GJB received honoraria for teaching from GE Healthcare at the time of this study. There are no other known conflicts of interest to disclose

Ethics:

This study was covered by the UK Multiple Sclerosis Tissue Bank approval (Research Ethics Committee reference number 08/MRE09/31).

Funding

This study was supported by Barts Charity (grant code # 468/1506). DLT is supported by the UCL Leonard Wolfson Experimental Neurology Centre (PR/ylr/18575), the Wellcome Trust (Centre award 539208) and the UCLH NIHR Biomedical Research Centre.

Authorship

All authors have made substantial contributions to 1) conception and design, or acquisition of data, or analysis and interpretation of data; 2) drafting the article or revising it critically for important intellectual content; and 3) final approval of the version to be published.

Abstract

Purpose: Validation of quantitative MR measures for myelin imaging in the post mortem Multiple Sclerosis (MS) spinal cord.

Methods: Four fixed spinal cord samples were imaged first with a 3T clinical MR scanner to identify areas of interest for scanning, and then with a 7T small bore scanner using a multicomponent driven equilibrium single pulse observation of T1 and T2 protocol to produce apparent proton density (aPD), T1, T2, myelin water, intra-cellular water and free water fraction maps. After imaging, the cords were sectioned and stained with histological markers (Haematoxylin & Eosin, Myelin Basic Protein and neurofilament protein), which were quantitatively compared to the MR maps.

Results: Excellent correspondence was found between high resolution MR parameter maps and histology, particularly for aPD MRI and Myelin Basic Protein staining.

Conclusion: High resolution quantitative MR imaging of the spinal cord provides biologically meaningful measures, and could be beneficial to diagnose and track MS lesions in the spinal cord.

Keywords: myelin water fraction, spinal cord, multiple sclerosis

Introduction

The myelin sheath is an extended and modified plasma membrane wrapped around axons in a spiral fashion[1]. Myelin is composed of about 40% water, whilst the dry mass consist of about 80% lipids, mainly the glycolipid galactocerebroside, and 20% protein[2]. Due to its importance for normal function of the nervous system, and severe consequences of myelin damage in demyelinating diseases, such as multiple sclerosis (MS), the non-invasive in vivo assessment of myelin remains a key focus of imaging research, not least in the era of regenerative medicine[3].

The spinal cord is most commonly affected in people with MS (pwMS) at presentation[4,5]. Lesions in the spinal cord have been shown to predict both a diagnosis of MS in patients with radiologically isolated, as well as clinically isolated, syndromes of demyelination (RIS, CIS)[6,7]; they are also associated with more severe disability[6,8]. As MS evolves over time, much of the permanent and deteriorating disability in people with MS affects lower body functions, including lack of sphincter control, sexual dysfunction, and impaired leg movement and coordination, resembling the clinical syndrome of progressive myelopathy[9-12]. Metrics such as spinal cord cross-sectional area (CSA) have been shown to be associated with MS- related disability in vivo[13]. However, CSA is affected by numerous elements of MS pathology including inflammation, edema, myelin content, the number of axons and gliosis.

MRI is widely used in the assessment of MS, but standard qualitative T1- and T2-weighted images are largely non-specific for the underlying pathology[14]. Quantitative MRI (qMRI) has the potential to distinguish specific tissue features, such as separating

demyelination from axonal loss[15]. Multi-Component relaxometry is a family of methods that can quantify the fractional amount of water in different tissue environments by exploiting the differences in relaxation time values. In the nervous system, these environments include free water in cerebrospinal fluid (CSF), intra- and extra-cellular water (IEW) and, most importantly in the context of demyelinating diseases, water 'trapped' between the myelin bilayers. The ratio of myelin water signal to total water signal is termed myelin water fraction (MWF)[16].

Along with other related quantitative measures, including the relaxation times themselves, MWF has shown promise to identify specific features of MS pathology and monitoring disease progression[17,18]. The gold-standard method for evaluating the MWF is analysis of a Multi-Echo T2 (MET2) relaxation curve[16]. The MET2 method has been previously compared to histology in *post mortem* brain at 1.5T[19], and Laule and coworkers demonstrated strong correlation of MWF in MS tissue samples at 7T with luxol fast blue (LFB) staining intensity for myelin on histology[20]. These studies support the hypothesis that myelin can be mapped in the brain using MWF. However, clinical translation of MET2 has been hampered by the long acquisition time required[21].

In contrast, gradient echo based methods, such as the Driven Equilibrium Single-Pulse Observation of T1 & T2 (DESPOT1&2), are inherently fast[22]. A multi-component version (mcDESPOT) has been used in clinical studies of MS[23], primary lateral sclerosis[24] and monitoring myelin development in children[25-29]. However, histological validation has been lacking, and recent work has shown that mcDESPOT suffers from unpredictable bias but as there was sufficient data for analysis we present it here[30,31].

Given significant efforts in MS research are directed towards development of strategies for myelin repair (remyelination)[32], imaging biomarkers of myelin are desirable. To establish whether mcDESPOT could provide such an index (or indices) we undertook correlative experiments using post mortem spinal cord, to quantitatively compare MRI and histology data.

Methods

Formalin-fixed spinal cords were placed on a Perspex frame and inserted into glass tubes. The formalin was drained and the tubes then filled with perfluoropolyether (Fomblin, Solvay Solutions UK Ltd) to provide a susceptibility-matched signal-free background (Supporting Information Figure S1).

Qualitative structural MRI was performed on the whole cords at 3T (Achieva Tx, Philips Healthcare, Best, Netherlands) using a 15 element SENSE Spine coil and a Turbo Spin Echo (TSE) sequence with the following parameters: echo time (TE) 16ms, repetition time (TR) 5000ms, voxel size 0.4x0.4x2.0mm^3). Nine areas of interest were identified by a neurologist with >20 years of experience in reading MRI of pwMS (KS) for scanning at 7T. The thoracic level 1 was marked with a radiologically opaque marker tied to the nerve root; measurements of distance from the marker for each lesion were noted and used to inform positioning of the glass tube for subsequent 7T scanning.

Next, the cords were scanned using a 7T pre-clinical scanner (Agilent Technologies, Santa Clara, California, USA) and 39-mm diameter quadrature transmit-receive RF coil (Rapid Biomedical GmbH, Rimpar, Germany) designed for whole-body rodent imaging. As the human spine is longer than the achievable field-of-view (FOV) with this setup, for each area of interest the glass tubes were moved in or out of the RF coil as required to place the desired area at both the centre of the RF coil and the isocentre of the magnet. We observed that the active area of the RF coil was longer than the linear region of the image encoding gradients. As the samples were long enough to protrude

into this region, protons that were excited by the RF but not encoded by the gradients resulted in a "zipper artefact" in some images. This was minimised by careful rotation of the samples so that the artefacts did not intrude into areas required for analysis. In most samples a small quantity of formalin remained after draining which produced bright signal at the top of the sample tube. To avoid this wrapping into the tissue the FoV was increased in the vertical direction.

Spoiled gradient echo (SPGR) and balanced steady-state free precession (bSSFP) (with 2 RF phase-cycles) sequences were acquired with the parameters given in Table 1, along with an Actual Flip Angle (AFI) acquisition for B_1 correction[33]. Images were resampled to 150x150x300µm^3 for processing. The images were processed using the open-source Quantitative Imaging Tools (QUIT) C++ toolbox[34] (available from http://github.com/spinicist/QUIT). T1 maps were generated using non-linear least squares fitting to images with all flip angles[35,36], and T2 and apparent Proton Density (aPD) maps were generated using the DESPOT2-FM method[37].

Calculation of MWF from mcDESPOT requires the a-priori specification of valid initial ranges of T1 and T2 for each water component[30,38]. It has been recognized that in post-mortem tissue these relaxation times change following fixation[39-41]. The single-component T1 and T2 of white matter in a healthy cord was used as a reference point for the myelin water T1 and T2, healthy grey matter relaxation times were used as reference points for the intra-/extra-cellular water T1 and T2, and literature values were used for the free-water fraction[38]. Fitting parameters including the ranges used for each water component are shown in Table 2. Non-overlapping ranges that

encompassed the reference points or literature values for these parameters were used. It has been shown that neglecting the effect of TE in the SPGR and bSSFP signal models lead to large errors in derived MWF values, so the echo-time corrected signal model was used[42].

MR parameter maps were then matched with histology using positional information (cord level and distance of the lesion from the marker) from the 3T whole cord scans, and checked against anatomical features (such as lesion shape and grey matter anatomy) in the histology and 7T images. MIPAV (http://mipav.cit.nih.gov/) was used to manually define ROIs on aPD maps and transfer them to all other maps for ROI analysis.

For histology, cords were dissected axially into blocks of 5mm thickness. Each tissue block was then marked with tissue dye to retain information on its spatial orientation and processed for embedding in paraffin. 10μm thick sections were cut from each tissue block using a Shandon Finesse ME1 microtome (Thermo-Scientific, UK. Care was taken to cut the sections in a plane perpendicular to the anterior spinal artery. The sections were mounted on Superfrost1 slides (VWR, UK) and left in a 608C oven overnight.

Serial sections of each block were stained for haematoxylin and eosin (H&E), phosphorylated neurofilaments (SMI-31, mouse monoclonal, 1:1000, Abcam, UK) and myelin basic protein (MBP, SMI-94, mouse monoclonal, 1:100, Covance, Princeton, NJ, USA) following a modified protocol [43-45].

Focal areas of complete myelin loss were identified on MBP immuno-stained sections as demyelinated lesions in the white (WML) and grey matter (GML). Cellularity and axonal counts were determined by counting the number of cells in four square ROIs (size: 120×120μm^2) cast randomly onto WML and non-lesional white matter (NLWM) on H&E and SMI-31 stained sections respectively (Supporting Information Figure S2). Cellularity and axonal counts were expressed as cells/mm^2 and axons/mm^2 respectively. Unpaired two-tailed t-tests were performed to compare MWF, IEWF and FWF values in the NLWM and WML ROIs.

Results

Formalin-fixed spinal cords of three pwMS (one male, two female), and one male control subject with no neurological disease were used. The MS cords were from donors who died at the age of 67-87 years. Their disease duration had been 8-44 years. The MS cords had been fixed for 1127-1441 days. The control subject died aged 89 years. Duration of fixation of this cord was 1366 days.

Figure 1 shows matched histology and quantitative MR parameter maps of spinal cords from the three MS patients and one control subject. Excellent visual correspondence was observed between the anatomic detail on histology images and aPD maps. Both T1 and T2 maps showed less contrast between lesion and healthy tissue than aPD, while the MWF produced high contrast, matching well with the myelin histology in the cords from pwMS. The IEWF map showed, as expected, the inverse of the MWF map (lower in myelinated areas and higher elsewhere). Surprisingly, the FWF map was non-zero in healthy tissue area especially in the control cords but decreased to zero in lesion areas. Cord MS454 had no grey matter areas that could definitely be determined as normal appearing grey matter. MBP staining, aPD, MWF, IEWF, and FWF images only are shown together in Supporting Information Figure S3 to facilitate comparison of the maps.

Quantitative histology results and mean values of the MR parameters from the ROIs are given in Table 3. Cellularity and axon count and MBP staining fraction were reduced in lesions compared to normal white-matter; MWF also showed a decrease in lesion areas, while the IEWF increased. We observed a noticeable decrease in the FWF fraction. It should be noted that the MBP staining fraction can only be compared

within a single batch, and hence there is variable staining between the pathological cords and the control cord, which was stained at a later date. Therefore, the MBP values were not entered into the correlation analysis for the control cord.

Graphs of the MWF, IEWF and FWF values in the NLWM, NLGM and WM and GM lesion are shown in Supporting Information Figure S4. MWF, IEWF and FWF were all significantly different between NLWM and WML ($P < 0.0001$). Graphs of correlation (Pearson's correlation) between histological and MR indices over all white matter lesions and non-lesional white matter in MS cords, and control white matter in control cords (axon counts vs. aPD, T1, MWF, and MBP stain vs. T1, MWF) are shown in Figure 2. All are significant (Pearson's R and P-values shown on graphs and tabled in Supporting Information Table S1). Correlations between MWF and aPD in individual white matter types (WML, NLWM and control WM) and histological indices are shown in Supporting Information Figure S5 and S6 respectively. Correlation between both cell nuclei and axon counts and MWF in WML were not significant. Correlation between nuclei counts and MWF in NLWM and control WM was just significant ($P=0.046$), but not significant between axons and MWF in NLWM and control WM. This significance is likely due to the difference in nuclei between control data and NLWM rather than a correlation with MWF.

Discussion

Our results show that with high resolution scanning at 7T, good correspondence between qMRI and histological metrics is observed. aPD maps show excellent contrast between healthy and pathological tissue, and T1 & T2 maps provide quantitative measures that correlate with quantitative histology measures.

The myelin water fraction (MWF) maps show clear differentiation between lesion and non-lesional tissue. The non-zero FWF in the healthy control cord is an unexpected finding, as fixed tissue has not been thought to contain water protons with a long T2. This may indicate infiltration by the fixative or may simply be due to bias in the fitting procedure[31]. The FWF component in the control cords displays better contrast between WM and GM than the MWF for instance, which could be caused by either of these mechanisms. The measured FWF is lower in lesions in pathological cords, which may also be due to said bias or could indicate the assumption that the FWF is non-exchanging, i.e. that water cannot move between the FWF and IE-water pools, is invalid. In lesions it is possible that biological barriers between these pools break down such that they behave as one, with a common T1 and T2.

Our samples were not rinsed of fixative before acquisition as this could cause degradation of the tissue, and therefore contained formaldehyde. Formaldehyde causes known shortening of the T1 and T2 values reducing the differences between the myelin and intra-/extra-cellular compartments[46]. The stochastic region contraction (SRC) search algorithm used in mcDESPOT may not be able to consistently differentiate the signal from the different water pools in this situation. Care was taken

to choose appropriate fitting ranges (see Table 2), but derived MWF values are highly dependent on the selected parameter ranges, especially when the SRC algorithm is used for fitting[31,47]. An alternate approach such as the Bayesian priors of Bouhrara et al. may improve fitting accuracy[48]. Unfixed tissue is challenging to scan in a suitable time frame after death in humans and may show decomposition over a long scan time but, if possible, further validation in unfixed tissue would be desirable as the water pools should exhibit similar separation as in-vivo tissue.

The IEWF maps also show good definition between tissue types, with high values in lesional tissue. This implies more space in larger cells and between the cells in these areas. This has been postulated previously by Christiansen et al.[49], who found the apparent diffusion coefficient increased in MS lesions and suggested that this may be related to an increase in the extracellular space due to oedema and demyelination. They hypothesised the myelin removed is replaced by water resulting in an increase of the extracellular space and thereby the formerly restricted diffusion becomes less restricted.

Despite the issues related to fitting the mcDESPOT model, the MWF and IEWF showed good contrast and anatomic correspondence to the histology images, while the single component T1 and T2 maps showed comparatively low contrast. However, the aPD maps also show excellent correspondence with histology, with increased values in lesion areas. It should be noted that the because MWF and IEWF are defined as fractions, the aPD is effectively removed from the mcDESPOT measures; hence, the contrast in the aPD maps is orthogonal information to that in the mcDESPOT

parameter maps. Our results imply that if, for example, only the MWF is considered then an important additional source of information, namely the total water content in a voxel, will be missed.

Conclusion

High resolution quantitative MR parameter maps offer an alternative modality to histology for ex vivo quantitative assessment of MS spinal cord lesions. MWF maps showed good contrast between lesional and non-lesional tissue. Proton density, which reflects total water content, correlated significantly in MS lesions and offers additional information compared to the mcDESPOT parameter maps. The mcDESPOT model may benefit from the use of a Bayesian priors algorithm for more challenging conditions.

Table Captions

Table 1

MRI sequence acquisition parameters

Table 2

The minimum and maximum values that were set for T1 and T2 of each component during mcDESPOT fitting. The expected T1 and T2 of myelin and intra-/extra-cellular water were set significantly lower than for an equivalent in-vivo experiment because of formalin fixation is known to shorten these values. Fraction constraints constrain the MWF and FWF to within expected values to prevent convergence to an erroneous local minima. Myelin residence time is the mean time a water molecule stays in the myelin pool before exchanging to the IE-pool.

SPGR = Spoiled Gradient echo; bSSFP = Steady-State Free Precession; AFI = Actual Flip Angle

Table 3

Histology and MR indices for each region of interest. There are no lesions in the control cords. Hence, these entries are marked not applicable (NA). All three histology measures were reduced in lesions compared to normal white-matter. WML= white matter lesion; NLWM= non-lesional white matter.

MWF = Myelin Water Fraction; IEWF = Intra/Extra- cellular Water Fraction; FWF = Free Water Fraction

Table 1

Sequence	TE/TR [ms]	Flip-Angles	Voxel Size [μm³]	Matrix Size
SPGR	11.3/25	6, 8, 10, 15, 20, 25, 35, 45	100x125x200	160x160x160
bSSFP	2/4	14, 17, 20, 25, 35, 50, 65	100x125x200	160x160x160
AFI	2.62/7.5	55	250x250x500	64x64x64

Table 2

	MWF	IEW	FWF
T1 [ms]	50-350	400-800	1000-5000
T2 [ms]	8-14	14-25	200-1500
Fraction constraints [%]	0.1-50	NA	0.1-99
Myelin residence time [ms]	10 – 250	NA	NA

Table 3

Sample	MBP Stain %		Nuclei/mm²		Axons/mm²		APD (Arb Units)		T1 [ms]		T2 [ms]		MWF %		IEF %		FWF %	
	WML	NLWM	WML	NLWM	WML	NLWM	WML	NLWM	WML	NLWM	WML	NLWM	WML	NLWM	WML	NLWM	WML	NLWM
MS1 C8	1.78	83.92	1736	1858	7969	20174	6.0E+05	4.5E+05	708.3	445.3	21.4	16	3.6	18.5	96.2	80.4	0.2	1.2
MS1 T3	5.17	78.56	1458	2546	8767	14601	4.9E+05	3.4E+05	518.9	390.6	17.4	14.7	14.1	28.1	85.3	69.7	0.6	2.3
MS1 T5	3.35	87.86	1892	1944	2326	11782	6.1E+05	4.1E+05	604.3	407.2	19.8	15.4	8.7	23.3	91	74.4	0.3	2.3
MS1 T11	1.9	88.31	2760	2778	9514	15122	5.8E+05	4.2E+05	590.9	394.9	19.5	15.2	9	24.9	90.8	76.7	0.2	4.8
MS2 T11	2.89	63.4	2170	2135	7934	12604	5.6E+05	4.2E+05	578.2	517.4	17.4	17.5	13	14.8	86	83	1	2.2
MS3 C07A	15.71	61.46	1215	1615	8281	18843	5.4E+05	4.2E+05	663.6	449.7	18.4	15.4	5.5	23	93.8	75.7	0.7	1.3
MS3 C07B	0.59	43.39	1233	1389	7639	15625	5.1E+05	5.0E+05	634.7	478.9	19.1	15.5	7	18.2	92.6	79.8	0.4	2
Control C7	NA	73.91	NA	27018	NA	15634	NA	4.5E+05	NA	403.5	NA	13.9	NA	29.8	NA	67.1	NA	3.1
Control T8	NA	44.47	NA	27456	NA	16571	NA	4.4E+05	NA	410.4	NA	14.3	NA	29.1	NA	68.5	NA	2.5

Figure captions

Figure 1

Histology and MR maps of three MS spinal cords, from top to bottom, sections taken from spinal cord 1 at levels C8, T3, T5 and T11, spinal cord 2 at T11 and spinal cord 3, two lesions at C7. Control cord sections at C8 and T9 are shown on the bottom two rows. The histological slides stained with MBP, H&E and SMI at the level of each lesion found are shown next to aPD, T1, T2, MWF, IEF and FWF maps at the same level. From left to right: MBP, H&E, SMI stained sections, aPD, T1, T2, MWF, IEWF and FWF. All images were scaled between identical limits for each contrast so a comparison could be made (aPD 0 - 5.0x10^5 PU; T1 0 - 800 ms; T2 10 - 20 ms; MWF 0 - 0.5 %; IEWF 0 - 1 %; FWF 0 - 0.05 %) MWF = Myelin Water Fraction; IEWF = Intra/Extra- cellular Water Fraction; FWF = Free Water Fraction

Figure 2

Correlation between histological and MR indices over all white matter lesion, and non-lesional white matter in MS cords and control white matter in control cords. Correlation of axons against aPD, T1 and myelin water fraction (A, B and C respectively) and MBP against aPD and T1 (D and E respectively). Control cord white matter data is shown by the red data points, non-lesional white matter by black dots, and lesional white matter by green dots. The best fit line is shown with 95% confidence intervals. R = Person's R value and P = P-value

Figures

Figure 1

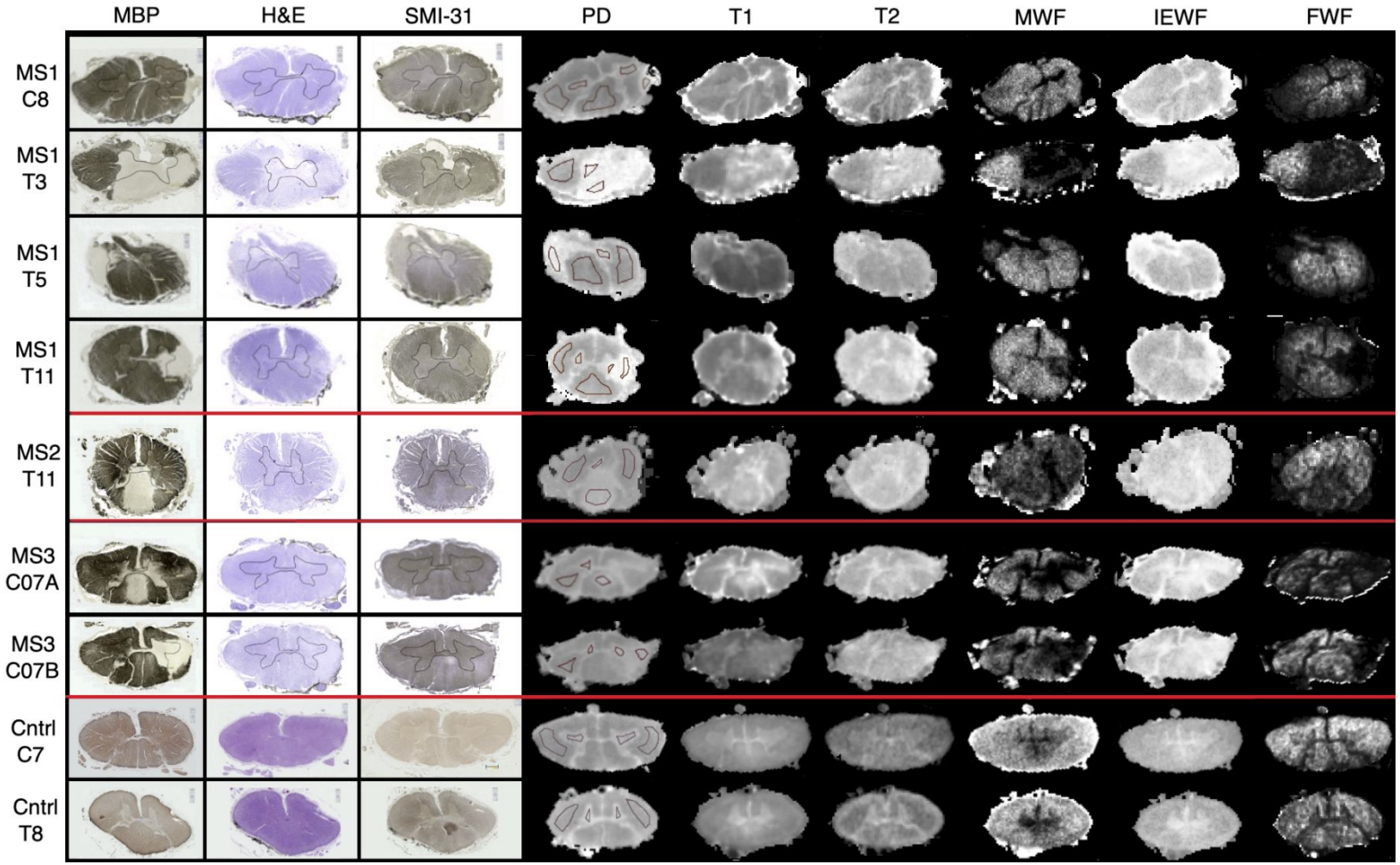

Figure 2

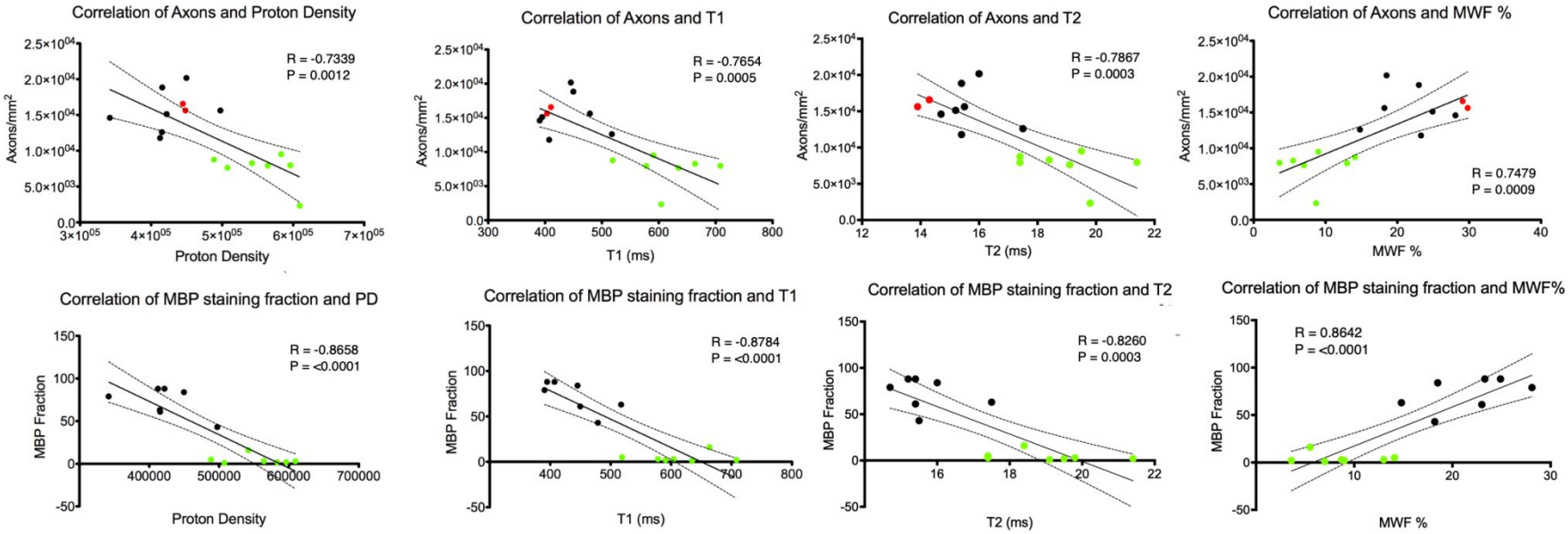
Correlation of Axons and Proton Density
R = -0.7339
P = 0.0012
Axons/mm2
Proton Density
Correlation of Axons and T1
R = -0.7654
P = 0.0005
Axons/mm2
T1 (ms)
Correlation of Axons and T2
R = -0.7867
P = 0.0003
Axons/mm2
T2 (ms)
Correlation of Axons and MWF %
R = 0.7479
P = 0.0009
Axons/mm2
MWF %
Correlation of MBP staining fraction and PD
R = -0.8658
P = <0.0001
MBP Fraction
Proton Density
Correlation of MBP staining fraction and T1
R = -0.8784
P = <0.0001
MBP Fraction
T1 (ms)
Correlation of MBP staining fraction and T2
R = -0.8260
P = 0.0003
MBP Fraction
T2 (ms)
Correlation of MBP staining fraction and MWF%
R = 0.8642
P = <0.0001
MBP Fraction
MWF %

References

1. Raine CS. Morphology of Myelin and Myelination. In: Morell P, ed. *Myelin.* Boston, MA: Springer US; 1984:1-50.
2. Morell P, Quarles RH. The Myelin Sheath. In: Siegel GJ, Agranoff BW, Albers RW, eds. *Basic Neurochemistry: Molecular, Cellular and Medical Aspects.* Philadelphia: Lippincott-Raven; 1999.
3. Neumann B, Foerster S, Zhao C, et al. Problems and Pitfalls of Identifying Remyelination in Multiple Sclerosis. *Cell Stem Cell.* 2020;26(5):617-619.
4. Katz Sand I. Classification, diagnosis, and differential diagnosis of multiple sclerosis. *Current opinion in neurology.* 2015;28(3):193-205.
5. Mowry EM, Pesic M, Grimes B, Deen S, Bacchetti P, Waubant E. Demyelinating events in early multiple sclerosis have inherent severity and recovery. *Neurology.* 2009;72(7):602-608.
6. Arrambide G, Rovira A, Sastre-Garriga J, et al. Spinal cord lesions: A modest contributor to diagnosis in clinically isolated syndromes but a relevant prognostic factor. *Multiple sclerosis (Houndmills, Basingstoke, England).* 2018;24(3):301-312.
7. Okuda DT, Mowry EM, Cree BAC, et al. Asymptomatic spinal cord lesions predict disease progression in radiologically isolated syndrome. *Neurology.* 2011;76(8):686.
8. Brownlee WJ, Altmann DR, Alves Da Mota P, et al. Association of asymptomatic spinal cord lesions and atrophy with disability 5 years after a clinically isolated syndrome. *Multiple sclerosis (Houndmills, Basingstoke, England).* 2017;23(5):665-674.
9. Giovannoni G, Cutter G, Sormani MP, et al. Is multiple sclerosis a length-dependent central axonopathy? The case for therapeutic lag and the asynchronous progressive MS hypotheses. *Mult Scler Relat Disord.* 2017;12:70-78.
10. Kearney H, Miller DH, Ciccarelli O. Spinal cord MRI in multiple sclerosis--diagnostic, prognostic and clinical value. *Nature reviews Neurology.* 2015;11(6):327-338.
11. Kremenchutzky M, Rice GP, Baskerville J, Wingerchuk DM, Ebers GC. The natural history of multiple sclerosis: a geographically based study 9: observations on the progressive phase of the disease. *Brain : a journal of neurology.* 2006;129(Pt 3):584-594.
12. McDonald I, Compston A. Chapter 6 - The symptoms and signs of multiple sclerosis. In: Compston A, Confavreux C, Lassmann H, et al., eds. *McAlpine's Multiple Sclerosis (Fourth Edition).* Edinburgh: Churchill Livingstone; 2006:287-346.
13. Losseff NA, Webb SL, O'Riordan JI, et al. Spinal cord atrophy and disability in multiple sclerosis. A new reproducible and sensitive MRI method with potential to monitor disease progression. *Brain : a journal of neurology.* 1996;119 (Pt 3):701-708.
14. Giorgio A, De Stefano N. Effective Utilization of MRI in the Diagnosis and Management of Multiple Sclerosis. *Neurologic clinics.* 2018;36(1):27-34.

15. Schmierer K, McDowell A, Petrova N, Carassiti D, Thomas DL, Miquel ME. Quantifying multiple sclerosis pathology in post mortem spinal cord using MRI. *NeuroImage.* 2018;182:251-258.
16. MacKay A, Whittall K, Adler J, Li D, Paty D, Graeb D. In vivo visualization of myelin water in brain by magnetic resonance. *Magnetic resonance in medicine.* 1994;31(6):673-677.
17. Vavasour IM, Laule C, Li DK, et al. Longitudinal changes in myelin water fraction in two MS patients with active disease. *Journal of the neurological sciences.* 2009;276(1-2):49-53.
18. MacKay AL, Vavasour IM, Rauscher A, et al. MR relaxation in multiple sclerosis. *Neuroimaging clinics of North America.* 2009;19(1):1-26.
19. Moore GR, Leung E, MacKay AL, et al. A pathology-MRI study of the short-T2 component in formalin-fixed multiple sclerosis brain. *Neurology.* 2000;55(10):1506-1510.
20. Laule C, Kozlowski P, Leung E, Li DK, Mackay AL, Moore GR. Myelin water imaging of multiple sclerosis at 7 T: correlations with histopathology. *NeuroImage.* 2008;40(4):1575-1580.
21. Ljungberg E, Vavasour I, Tam R, et al. Rapid myelin water imaging in human cervical spinal cord. *Magnetic resonance in medicine.* 2017;78(4):1482-1487.
22. Deoni SC, Rutt BK, Arun T, Pierpaoli C, Jones DK. Gleaning multicomponent T1 and T2 information from steady-state imaging data. *Magnetic resonance in medicine.* 2008;60(6):1372-1387.
23. Kitzler HH, Su J, Zeineh M, et al. Deficient MWF mapping in multiple sclerosis using 3D whole-brain multi-component relaxation MRI. *NeuroImage.* 2012;59(3):2670-2677.
24. Kolind S, Sharma R, Knight S, Johansen-Berg H, Talbot K, Turner MR. Myelin imaging in amyotrophic and primary lateral sclerosis. *Amyotrophic lateral sclerosis & frontotemporal degeneration.* 2013;14(7-8):562-573.
25. Deoni SC, Dean DC, 3rd, O'Muircheartaigh J, Dirks H, Jerskey BA. Investigating white matter development in infancy and early childhood using myelin water faction and relaxation time mapping. *NeuroImage.* 2012;63(3):1038-1053.
26. Deoni SC, Dean DC, 3rd, Piryatinsky I, et al. Breastfeeding and early white matter development: A cross-sectional study. *NeuroImage.* 2013;82:77-86.
27. Spader HS, Ellermeier A, O'Muircheartaigh J, et al. Advances in myelin imaging with potential clinical application to pediatric imaging. *Neurosurgical focus.* 2013;34(4):E9.
28. Miele A, Pan J, Walker L, et al. B-74The Relationship of Myelin Content and Measures of Executive Functioning in Typically Developing Children. *Archives of clinical neuropsychology : the official journal of the National Academy of Neuropsychologists.* 2014;29(6):564.
29. Miele A, Pan J, Walker L, et al. B-75Neural Correlates of Emerging Executive Functioning in 2-5 Year Olds. *Archives of clinical neuropsychology : the official journal of the National Academy of Neuropsychologists.* 2014;29(6):565.
30. Lankford CL, Does MD. On the inherent precision of mcDESPOT. *Magnetic resonance in medicine.* 2013;69(1):127-136.

31. West DJ, Teixeira R, Wood TC, Hajnal JV, Tournier JD, Malik SJ. Inherent and unpredictable bias in multi-component DESPOT myelin water fraction estimation. *NeuroImage.* 2019;195:78-88.
32. Cunniffe N, Coles A. Promoting remyelination in multiple sclerosis. *Journal of neurology.* 2021;268(1):30-44.
33. Yarnykh VL. Actual flip-angle imaging in the pulsed steady state: a method for rapid three-dimensional mapping of the transmitted radiofrequency field. *Magnetic resonance in medicine.* 2007;57(1):192-200.
34. Wood TC, Simmons C, Hurley SA, et al. Whole-brain ex-vivo quantitative MRI of the cuprizone mouse model. *PeerJ.* 2016;4:e2632.
35. Chang LC, Koay CG, Basser PJ, Pierpaoli C. Linear least-squares method for unbiased estimation of T1 from SPGR signals. *Magnetic resonance in medicine.* 2008;60(2):496-501.
36. Stikov N, Boudreau M, Levesque IR, Tardif CL, Barral JK, Pike GB. On the accuracy of T mapping: Searching for common ground. *Magnetic resonance in medicine.* 2014.
37. Deoni SC. Transverse relaxation time (T2) mapping in the brain with off-resonance correction using phase-cycled steady-state free precession imaging. *Journal of magnetic resonance imaging : JMRI.* 2009;30(2):411-417.
38. Deoni SC, Matthews L, Kolind SH. One component? Two components? Three? The effect of including a nonexchanging "free" water component in multicomponent driven equilibrium single pulse observation of T1 and T2. *Magnetic resonance in medicine.* 2013;70(1):147-154.
39. Tovi M, Ericsson A. Measurements of T1 and T2 over time in formalin-fixed human whole-brain specimens. *Acta radiologica (Stockholm, Sweden : 1987).* 1992;33(5):400-404.
40. Blamire AM, Rowe JG, Styles P, McDonald B. Optimising imaging parameters for post mortem MR imaging of the human brain. *Acta radiologica (Stockholm, Sweden : 1987).* 1999;40(6):593-597.
41. Schmierer K, Wheeler-Kingshott CA, Tozer DJ, et al. Quantitative magnetic resonance of postmortem multiple sclerosis brain before and after fixation. *Magnetic resonance in medicine.* 2008;59(2):268-277.
42. Bouhrara M, Spencer RG. Incorporation of nonzero echo times in the SPGR and bSSFP signal models used in mcDESPOT. *Magnetic resonance in medicine.* 2015;74(5):1227-1235.
43. Geurts JJ, Bo L, Pouwels PJ, Castelijns JA, Polman CH, Barkhof F. Cortical lesions in multiple sclerosis: combined postmortem MR imaging and histopathology. *AJNR American journal of neuroradiology.* 2005;26(3):572-577.
44. Tallantyre EC, Bo L, Al-Rawashdeh O, et al. Clinico-pathological evidence that axonal loss underlies disability in progressive multiple sclerosis. *Multiple sclerosis (Houndmills, Basingstoke, England).* 2010;16(4):406-411.
45. Petrova N, Carassiti D, Altmann DR, Baker D, Schmierer K. Axonal loss in the multiple sclerosis spinal cord revisited. *Brain pathology (Zurich, Switzerland).* 2018;28(3):334-348.
46. Seifert AC, Umphlett M, Hefti M, Fowkes M, Xu J. Formalin tissue fixation biases myelin-sensitive MRI. *Magnetic resonance in medicine.* 2019;82(4):1504-1517.

47. Bouhrara M, Reiter DA, Celik H, Fishbein KW, Kijowski R, Spencer RG. Analysis of mcDESPOT- and CPMG-derived parameter estimates for two-component nonexchanging systems. *Magnetic resonance in medicine.* 2016;75(6):2406-2420.
48. Bouhrara M, Spencer RG. Improved determination of the myelin water fraction in human brain using magnetic resonance imaging through Bayesian analysis of mcDESPOT. *NeuroImage.* 2015.
49. Christiansen P, Gideon P, Thomsen C, Stubgaard M, Henriksen O, Larsson HB. Increased water self-diffusion in chronic plaques and in apparently normal white matter in patients with multiple sclerosis. *Acta neurologica Scandinavica.* 1993;87(3):195-199.

Supporting Information

Supporting Information Figure S1 Caption

Whole spinal cord secured in a glass tube and immersed in perfluoropolyether ready for scanning.

Supporting Information Figure S2 Caption

Example H&E stained section (left, A) with four square ROIs positioned in the red outlined region (top right, B), grey matter is outlined in black. Zoomed section (bottom right, C) shows detail in square ROI. Cellularity and axonal counts were determined by counting the number of cells in four square ROIs (size: 120×120μm^2) cast onto lesional and non-lesional white matter on the H&E and SMI-31 stained sections.

Supporting Information Figure S3 Caption

Expanded Figure taken from Figure 2 showing only MDP, PD, MWF, IEWF and FWF to facilitate comparison

Supporting Information Figure S4 Caption

Box and whisker plots of all MR parameters in each tissue type. Red points are control samples, for which there is no lesional data. Differences in all parameters were present between NLWM and WM lesion. Centre line is the mean with whiskers of one standard deviation.

Supporting Information Table S1 Caption

Correlation coefficients for graphs shown in Figure 2

Supporting Information Figure S5 Caption

Graphs of correlation for myelin water fraction separated into individual white matter types expanded from Figure 2; white matter lesion and non-lesional white matter. Correlations with nuclei against myelin water fraction in white matter lesion and non-lesional white matter in MS cords and control white matter in control cords (A and C respectively) and axons against myelin water fraction in white matter lesion and non-lesional white matter in MS cords and control white matter in control cords (B and D respectively). Control cord white matter data is shown by the red data points. The best fit line is shown with the 95% confidence intervals.

Supporting Information Figure S6 Caption

Graphs of correlation for proton density separated into individual white matter types expanded from Figure 2; white matter lesion and non-lesional white matter. Correlations with nuclei against proton density in white matter lesion and non-lesional white matter in MS cords and control white matter in control cords (A and C respectively) and axons against proton density in white matter lesion and non-lesional white matter in MS cords and control white matter in control cords (B and D respectively). Control cord white matter data is shown by the red data points. The best fit line is shown with the 95% confidence intervals.

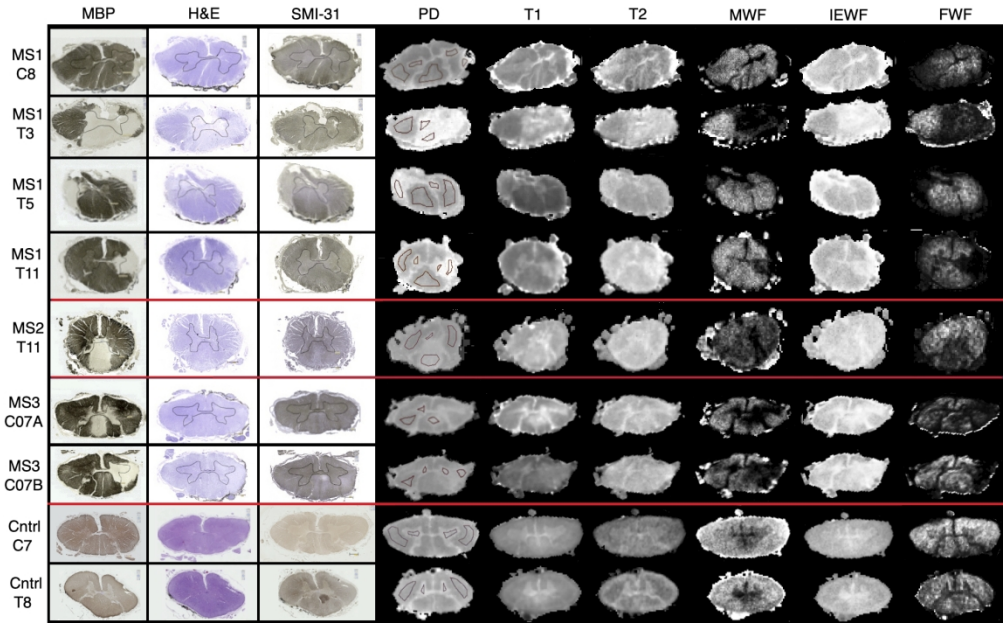

Histology and MR maps of three MS spinal cords, from top to bottom, sections taken from spinal cord 1 at levels C8, T3, T5 and T11, spinal cord 2 at T11 and spinal cord 3, two lesions at C7. Control cord sections at C8 and T9 are shown on the bottom two rows. The histological slides stained with MBP, H&E and SMI at the level of each lesion found are shown next to aPD, T1, T2, MWF, IEF and FWF maps at the same level. From left to right: MBP, H&E, SMI stained sections, aPD, T1, T2, MWF, IEWF and FWF. All images were scaled between identical limits for each contrast so a comparison could be made (aPD 0 - 5.0x105 PU; T1 0 - 800 ms; T2 10 - 20 ms; MWF 0 - 0.5 %; IEWF 0 - 1 %; FWF 0 - 0.05 %) MWF = Myelin Water Fraction; IEWF = Intra/Extra- cellular Water Fraction; FWF = Free Water Fraction

684x426mm (72 x 72 DPI)

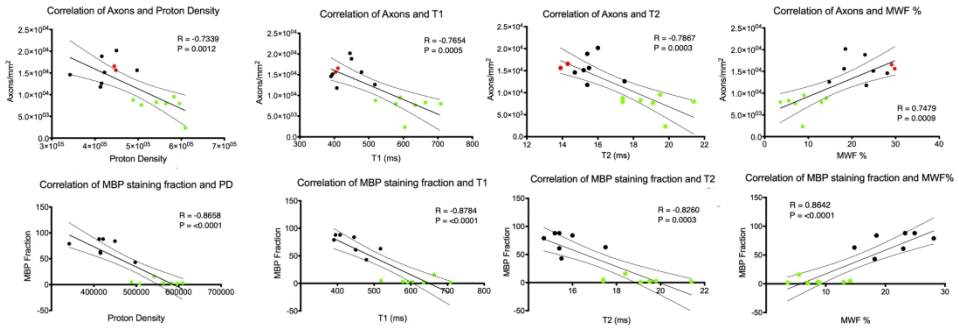

Correlation between histological and MR indices over all white matter lesion, and non-lesional white matter in MS cords and control white matter in control cords. Correlation of axons against aPD, T1 and myelin water fraction (A, B and C respectively) and MBP against aPD and T1 (D and E respectively). Control cord white matter data is shown by the red data points, non-lesional white matter by black dots, and lesional white matter by green dots. The best fit line is shown with 95% confidence intervals. R = Person's R value and P = P-value

889x335mm (72 x 72 DPI)

Supporting Information Figure S1

Supporting Information Figure S1 Caption

Whole spinal cord secured in a glass tube and immersed in perfluoropolyether ready for scanning.

Supporting Information Figure S2

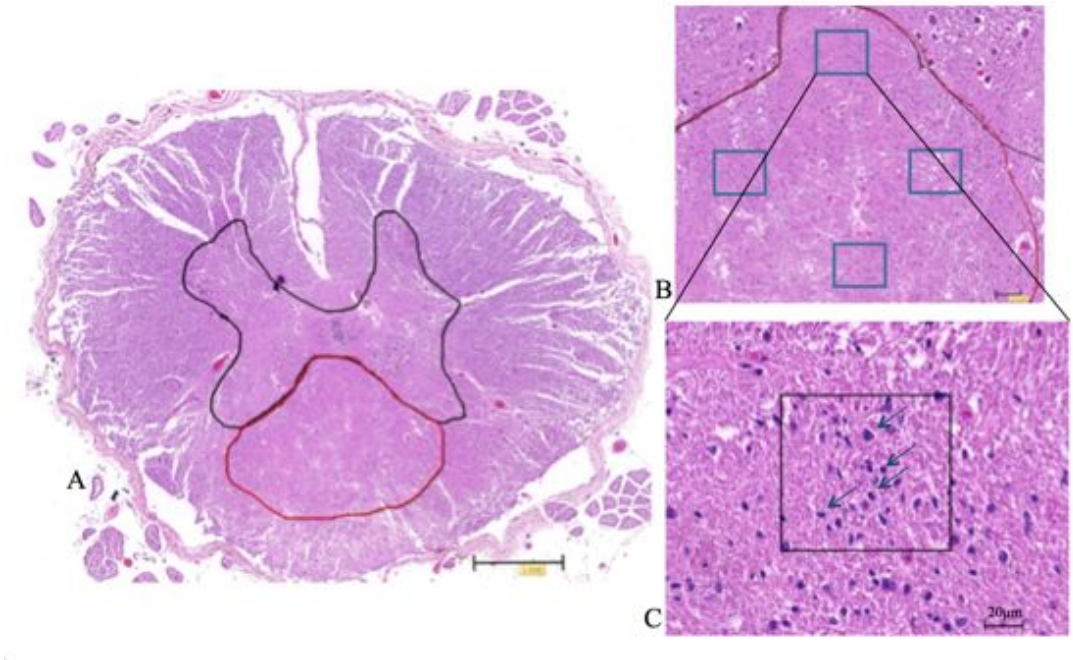

Supporting Information Figure S2 Caption

Example H&E stained section (left, A) with four square ROIs positioned in the red outlined region (top right, B), grey matter is outlined in black. Zoomed section (bottom right, C) shows detail in square ROI. Cellularity and axonal counts were determined by counting the number of cells in four square ROIs (size: 120×120μm^2) cast onto lesional and non-lesional white matter on the H&E and SMI-31 stained sections.

Supporting Information Figure S3

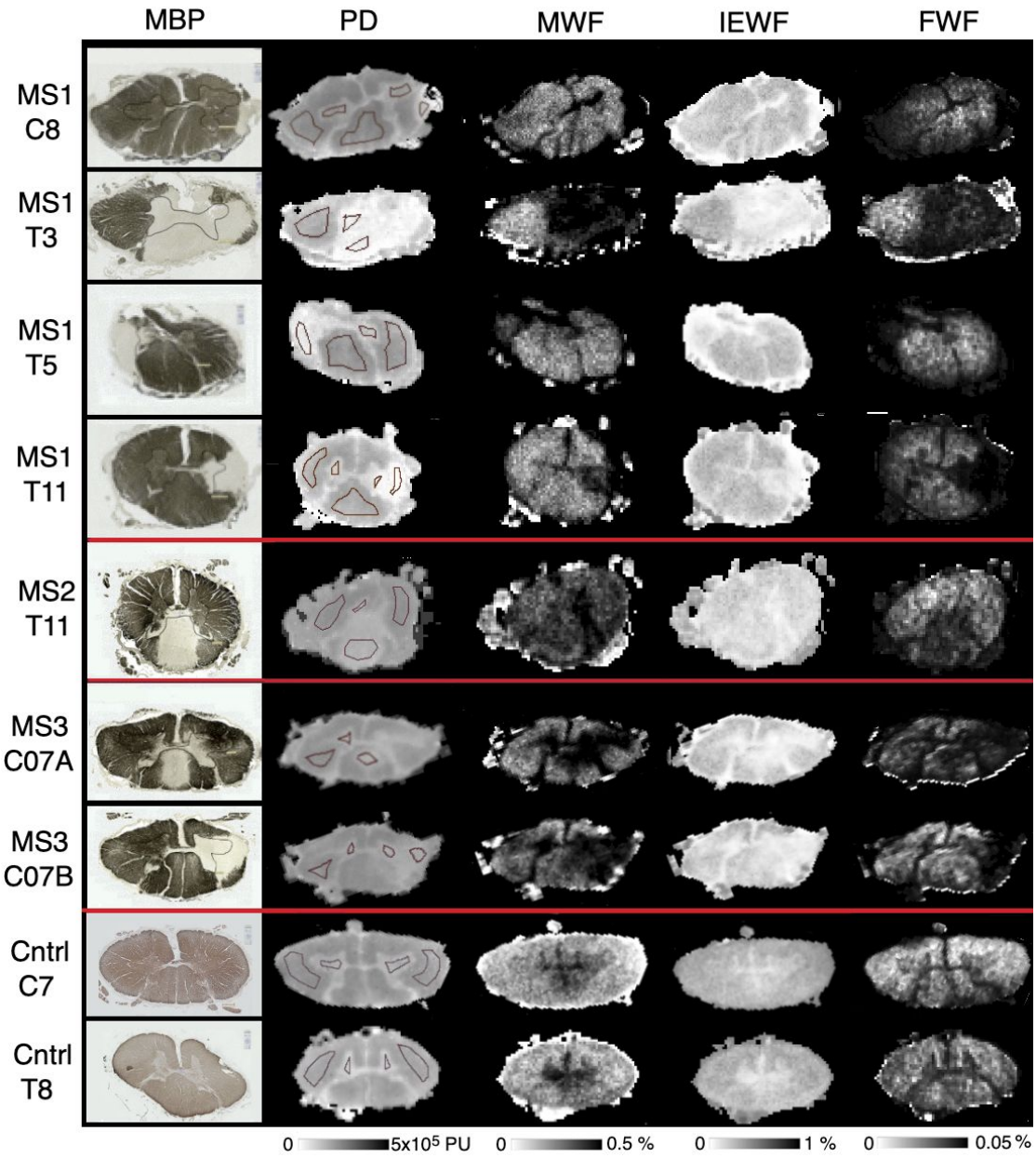

Supporting Information Figure S3 Caption

Expanded Figure taken from Figure 2 showing only MDP, PD, MWF, IEWF and FWF to facilitate comparison

Supporting Information Figure S4

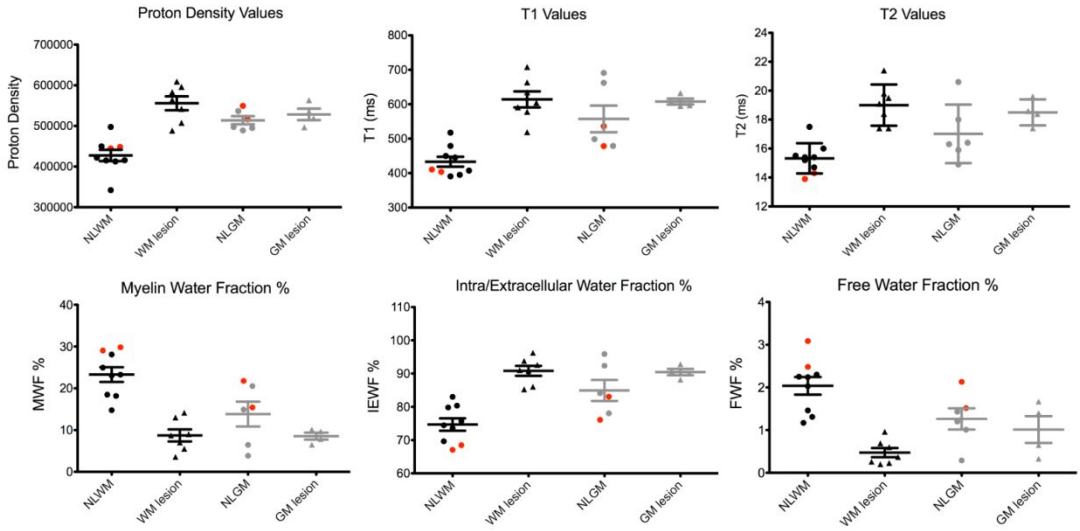

Supporting Information Figure S4 Caption

Box and whisker plots of all MR parameters in each tissue type. Red points are control samples, for which there is no lesional data. Differences in all parameters were present between NLWM and WM lesion. Centre line is the mean with whiskers of one standard deviation.

Supporting Information Table S1

HISTOLOGY	MR INDICES	R	P
AXONS	Proton Density	-0.7339	0.0012
	T1 (ms)	-0.7654	0.0005
	T2 (ms)	-0.7867	0.0003
	MWF (%)	0.7479	0.0009
MBP FRACTION	Proton Density	-0.8658	<0.0001
	T1 (ms)	-0.8784	<0.0001
	T2 (ms)	-0.8260	0.0003
	MWF (%)	0.8642	<0.0001

Supporting Information Table S1 Caption

Correlation coefficients for graphs shown in Figure 2

Supporting Information Figure S5

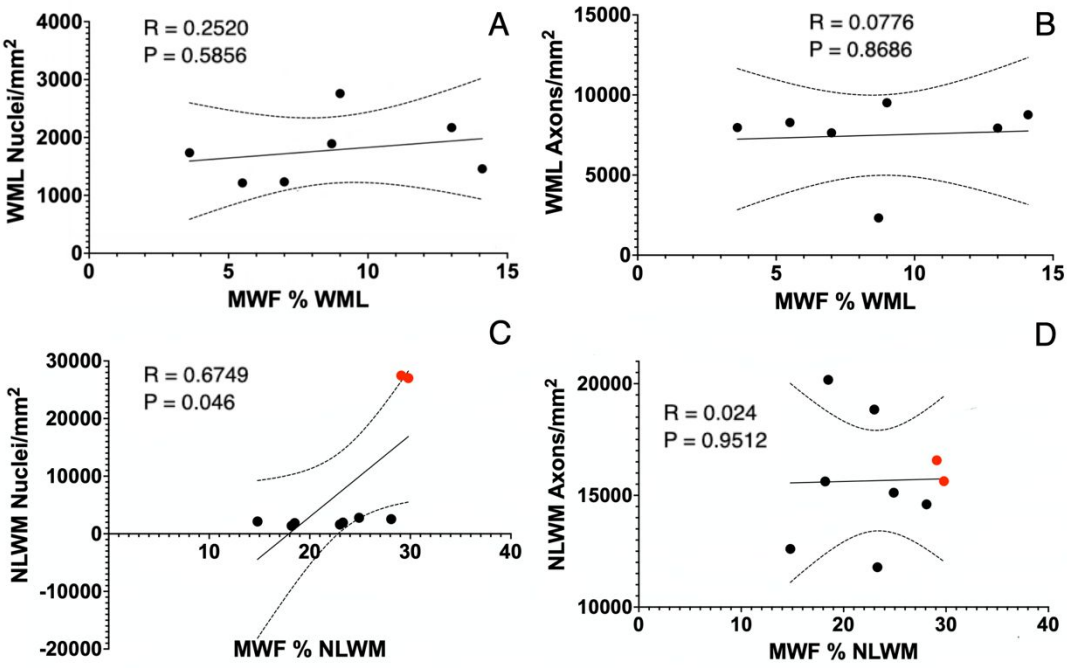

Supporting Information Figure S5 Caption

Graphs of correlation for myelin water fraction separated into individual white matter types expanded from Figure 2; white matter lesion and non-lesional white matter. Correlations with nuclei against myelin water fraction in white matter lesion and non-lesional white matter in MS cords and control white matter in control cords (A and C respectively) and axons against myelin water fraction in white matter lesion and non-lesional white matter in MS cords and control white matter in control cords (B and D respectively). Control cord white matter data is shown by the red data points. The best fit line is shown with the 95% confidence intervals.

Supporting Information Figure S6

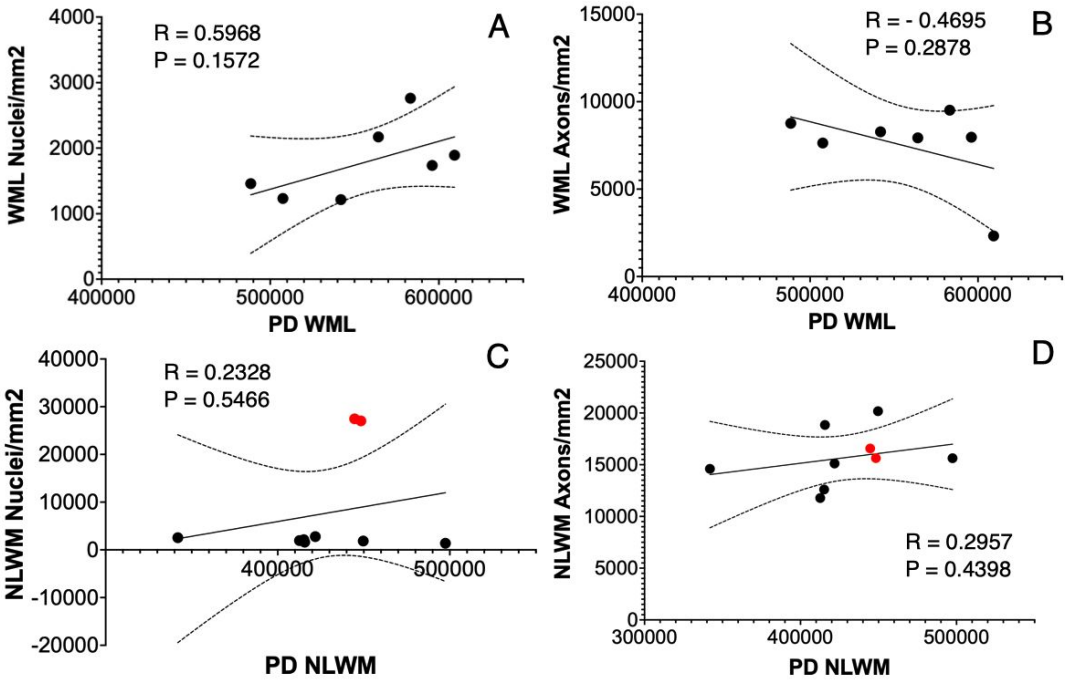

Supporting Information Figure S6 Caption

Graphs of correlation for proton density separated into individual white matter types expanded from Figure 2; white matter lesion and non-lesional white matter. There was no significant correlation for PD with histological indices in individual tissue types. Correlations with nuclei against proton density in white matter lesion and non-lesional white matter in MS cords and control white matter in control cords (A and C respectively) and axons against proton density in white matter lesion and non-lesional white matter in MS cords and control white matter in control cords (B and D respectively). Control cord white matter data is shown by the red data points. The best fit line is shown with the 95% confidence intervals.